RSC Advances

PAPER

View Article Online
View Journal | View Issue

Cite this: *RSC Adv.*, 2025, **15**, 24750

CO, H_2S, and NH_3 gas sensing on Mn-doped WSe_2 monolayers: a DFT and machine learning study

N. V. Hoang *[ab] and Tr. Q. Trieu[c]

The structural, electronic, magnetic, optical, and thermo-mechanical properties of Mn-doped WSe_2 (WSe_2Mn) monolayers and their CO-, H_2S-, and NH_3-adsorbed counterparts were systematically investigated using density functional theory and machine learning techniques. All systems exhibited spin-resolved semimetallic behavior, characterized by metallic spin-up and semiconducting spin-down channels. Magnetic ordering was maintained upon gas adsorption, with a slight enhancement in magnetic moment observed for the H_2S-adsorbed configuration. Thermo-mechanical analysis revealed that gas adsorption increases the bulk modulus and heat capacities while preserving the shear modulus, suggesting enhanced compressive stiffness without compromising shear resistance. The thermal expansion coefficient and Debye temperature showed gas-dependent variations, particularly under NH_3 exposure, indicating strong vibrational coupling. Optical calculations demonstrated strong absorption in the ultraviolet and partial visible range. These findings underscore the potential of WSe_2Mn monolayers for multifunctional applications in nanoelectronics, gas sensing, and thermally responsive devices.

Received 13th June 2025
Accepted 9th July 2025

DOI: 10.1039/d5ra04186d

rsc.li/rsc-advances

1. Introduction

Nanostructures play a crucial role in modern science and technology. Among them, two-dimensional (2D),[1–3] one-dimensional (1D),[4–6] and zero-dimensional (0D)[7–9] materials have been extensively investigated due to their distinct quantum confinement effects. Graphene, a single-layer 2D material,[10–12] is the basic structural unit of graphite,[13,14] carbon nanotubes,[15,16] and fullerenes.[17,18] Monolayer WSe_2, a prominent 2D semiconductor, exhibits a direct bandgap of ~1.566 eV, while its bulk form shows an indirect bandgap.[19–22] Its electronic properties are highly strain-sensitive, with a semiconductor-to-metal transition observed under ~−10% biaxial compressive strain. WSe_2 also demonstrates excellent performance in sub-5 nm field-effect transistors (FETs), where DFT studies emphasize the critical influence of metal–WSe_2 contacts on carrier mobility and ON-current characteristics.[23]

The chemical vapor deposition (CVD) growth of WSe_2 monolayers on silica substrates was systematically investigated by Bilu Liu *et al.*,[24] who demonstrated that the electrical behavior of WSe_2 (p-type or bipolar) strongly depends on the choice of metal contacts. In a separate work, Yang Gao *et al.* reported the rapid CVD growth of high-quality WSe_2 monolayers on Au substrates.[25] These monolayers exhibited excellent crystallinity and electrical performance, comparable to mechanically exfoliated samples. Density functional theory (DFT) calculations attributed this to the exothermic diffusion and low energy barriers for W and Se atom incorporation on Au surfaces.

Efforts to tailor the properties of WSe_2 through chemical doping have also been widely reported.[26–28] Eleonora Pavoni *et al.* studied vanadium (V) doping at various concentrations (1.4–11.2%) and found that V incorporation reduced the bandgap and significantly altered the electronic and optical properties, including shifts in absorption spectra relevant to optoelectronic applications.[29] Another study explored the effects of Mn, Fe, and V doping, identifying Mn and Fe as n-type and V as p-type dopants. The formation of impurity clusters was shown to weaken magnetic exchange interactions, leading to more dynamic magnetic behavior and underscoring the importance of controlling dopant distribution.[30]

Additionally, Antonia Kagkoura *et al.* investigated Co- and Ni-doped WSe_2 for electrocatalytic applications in sustainable energy technologies.[31] Both doped systems exhibited efficient catalytic activity toward the oxygen evolution reaction (OER), with overpotentials of 370 mV (Co) and 400 mV (Ni) at 10 mA cm^{-2}, and toward the hydrogen evolution reaction (HER), with potentials of −0.22 V (Co) and −0.20 V (Ni) at −10 mA cm^{-2}. The catalysts also demonstrated high stability and performance as cathodes in polymer electrolyte membrane water electrolyzers.

Recent studies have explored doping strategies to enhance the gas sensing performance of WSe_2-based materials.[32–34] For instance, Pt-doped WSe_2 has shown improved adsorption and sensitivity toward NO_2, CO_2, SO_2, and H_2, with significant

[a]*Atomic Molecular and Optical Physics Research Group, Institute for Advanced Study in Technology, Ton Duc Thang University, Ho Chi Minh City, Vietnam. E-mail: hoangvanngoc@tdtu.edu.vn*

[b]*Faculty of Electrical and Electronics Engineering, Ton Duc Thang University, Ho Chi Minh City, Vietnam*

[c]*Nam Dinh Teacher Training's College, Nam Dinh City, Nam Dinh Province, Vietnam*

bandgap reduction and strong binding energies.[33] Mo-doping has also been demonstrated to enhance CO_2, CH_4, and N_2O adsorption, with favorable charge transfer characteristics and efficient gas desorption at ambient conditions.[35] Additionally, Re-doped WSe_2 has exhibited selective adsorption toward C_2H_4, C_2H_2, and CO, as revealed by DFT combined with nonequilibrium Green's function analysis.[36] In addition to the aforementioned studies, many other research efforts have explored gas sensing based on materials, leading to promising applications in sensor technology.[37–41]

Despite the growing interest in doped WSe_2 for gas sensing, the specific potential of Mn-doped WSe_2 (WSe_2Mn) monolayers has received limited attention in the literature. The incorporation of Mn atoms into the WSe_2 lattice is expected to induce notable modifications in the electronic structure, magnetic properties, and chemical reactivity, which may enhance the interaction between the material surface and gas molecules. In this work, we present a detailed theoretical investigation of the electronic, magnetic, and gas adsorption properties of WSe_2Mn monolayers with a particular focus on the detection of CO, H_2S, and NH_3 gases-molecules of high environmental and industrial relevance. Our approach combines density functional theory (DFT) with crystal graph convolutional neural networks (CGCNN), a state-of-the-art machine learning technique, to both characterize the structural and electronic response of WSe_2Mn to gas adsorption and predict adsorption-related properties with enhanced efficiency and accuracy. This integrated DFT-ML framework enables not only high-fidelity simulations but also improved generalization in evaluating structure–property relationships, offering a robust platform for rapid materials screening. These findings provide new insights into high-performance 2D gas sensors and broaden the application scope of WSe_2-based materials in nanoscale sensing technologies.

2. Computational methods

In this study, a combination of density functional theory (DFT) and machine learning techniques was employed to investigate the structural, electronic, and thermo-mechanical properties of WSe_2Mn monolayers and their interaction with gas molecules (CO, H_2S, and NH_3).

All DFT calculations were performed using the Quantum ESPRESSO package, which implements plane-wave-based pseudopotential methods. The Perdew–Burke–Ernzerhof (PBE) functional within the generalized gradient approximation (GGA) was used to describe the exchange–correlation interaction. The projector augmented-wave (PAW) method was employed, and a kinetic energy cutoff of 50 Ry was chosen for the plane-wave basis set. To account for van der Waals interactions during gas adsorption, the Grimme-D2 dispersion correction scheme was applied. A vacuum layer of 20 Å was applied along the out-of-plane direction to prevent interaction between periodic images. Brillouin zone integration was carried out using a $11 \times 11 \times 1$ Monkhorst–Pack k-point mesh for geometry optimizations and force converged below thresholds of 10^{-7} Ry and 10^{-4} Ry $Bohr^{-1}$, respectively.

To investigate thermo-mechanical properties such as bulk modulus, shear modulus, heat capacities, thermal expansion coefficient, and Debye temperature, we employed the Crystal Graph Convolutional Neural Network (CGCNN) framework. The combination of DFT and CGCNN allows for comprehensive analysis of both the energetics and thermo-mechanical responses of WSe_2Mn monolayers under gas adsorption.

Adsorption energy is calculated by the formula:[42]

$$E_{AE} = E_T - E_P - E_M \quad (1)$$

In eqn (1), E_T, E_P, and E_M represent the total energies of the doped system, the pristine system, and the adsorbate molecule, respectively.

3. Results and discussion

3.1. Electromagnetic properties

The monolayer structure of WSe_2Mn and WSe_2Mn structures adsorbing $CO/H_2S/NH_3$ gas are shown in Fig. 1, WSe_2Mn has three atomic layers, the projection on the $x0y$ plane is a hexagonal structure. The structural parameters of WSe_2Mn and WSe_2Mn adsorbing $CO/H_2S/NH_3$ gas are shown in Table 1. The bond length between W–Se is d_1, d_1 has a value from 2.464 Å to 2.468 Å, these values are not significantly different, this result proves that the presence of $CO/H_2S/NH_3$ does not affect the W–Se distance much. Similar to d_1, d_2 and d_3 also vary in a very small range, d_2 has a value from 3.439 Å to 3.441 Å, while d_3 has a value from 3.011 Å to 3.021 Å, this result once again confirms that WSe_2Mn structure is less distorted when adsorbed by gas. When compared with structures similar to WSe_2Mn, such as monolayer MoS_2 with a bond length between Mo–S of 2.41 Å,[43] we see that the bond length between W–Se is about 0.05 Å larger, this result shows that there is not much difference, so the bonding force between W–Se in WSe_2Mn is almost similar to that between Mo–S in MoS_2. To see more clearly the strong or weak bond between atoms, we compare the bond length between W–Se with the bond length in the graphene structure, the bond length between C atoms in graphene is 1.42 Å,[44] which shows that the bond between C–C is stronger than the bond between W–Se.

The adsorption energy values for CO, H_2S, and NH_3 on WSe_2Mn monolayer are calculated to be −0.91 eV, −0.86 eV, and −0.96 eV, respectively. The negative adsorption energies indicate that all three gas adsorption processes are energetically favorable and exothermic. Among them, the NH_3 adsorption configuration exhibits the lowest adsorption energy, suggesting that NH_3 adsorption is the most thermodynamically favorable, making NH_3 more readily adsorbed onto WSe_2Mn surface compared to CO and H_2S.

Regarding the magnetic properties, both the pristine WSe_2Mn monolayer and its gas-adsorbed configurations exhibit magnetism, with total magnetic moments ranging from $2.670\mu_B$ to $2.175\mu_B$. Notably, the pristine WSe_2Mn and the NH_3-adsorbed WSe_2Mn configurations share the highest magnetic moment value. This result suggests that the adsorption of CO and H_2S leads to a slight reduction in the system's magnetic moment,

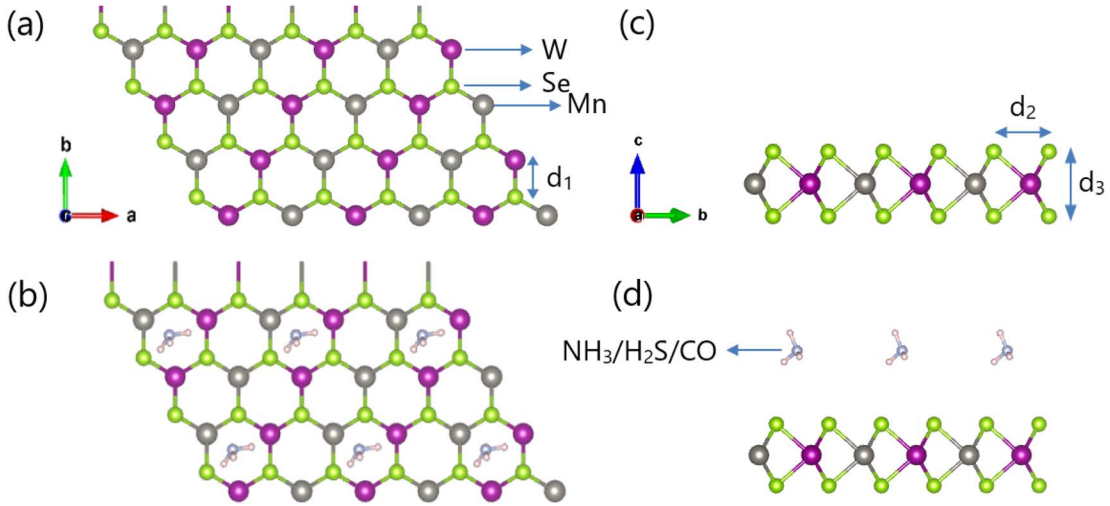

Fig. 1 Top view and side view of structures: (a and b) pristine WSe_2Mn monolayer, (c and d) $CO/H_2S/NH_3$-adsorbed WSe_2Mn monolayer (the atoms W, Se, Mn correspond to the colors purple, green and gray, respectively).

Table 1 Structural parameters of the WSe_2Mn monolayer before and after $CO/H_2S/NH_3$ gas adsorption (d_1 is the W–Se bond length, d_2 is the distance between two adjacent S atoms in the same plane, d_3 is the distance between two S atoms in two opposite planes)

Configurations	d_1 (Å)	d_2 (Å)	d_3 (Å)	E_a (eV)	μ (μ_B)
WSe_2Mn monolayer	2.465	3.439	3.011	—	2.175
CO adsorption	2.464	3.441	3.013	−0.91	2.174
H_2S adsorption	2.468	3.441	3.021	−0.86	2.670
NH_3 adsorption	2.465	3.439	3.013	−0.96	2.175

whereas NH_3 adsorption does not induce any significant change in the magnetic properties.

To investigate the impact of gas adsorption on the thermo-mechanical properties of the material, key parameters including the bulk modulus (B), shear modulus (G), constant-pressure heat capacity (C_p), constant-volume heat capacity (C_V), thermal expansion coefficient (α), and Debye temperature (T_D) were computed for WSe_2Mn system in both its pristine state and after the adsorption of CO, H_2S, and NH_3 gas molecules, employing the CGCNN method (Table 2). The results reveal that gas adsorption leads to an enhancement in the material's compressive modulus. Specifically, the bulk modulus increased from 17.36 GPa in the pristine system to 22.60 GPa (CO), 22.41 GPa (H_2S), and 21.28 GPa (NH_3), respectively. This increase indicates a trend toward structural stiffening induced by the interaction between gas molecules and WSe_2Mn monolayer, thereby improving the system's compressive strength. In contrast, the shear modulus (G) exhibits negligible variation, remaining in the range of 25.8–26.3 GPa, suggesting that the resistance to shear deformation is largely preserved following gas adsorption.

Regarding thermal properties, both the constant-pressure heat capacity (C_p) and constant-volume heat capacity (C_V) exhibited a slight increase following gas adsorption. Specifically, C_p increased from 2.93 k_B per atom in the pristine system to 2.96–2.99 k_B per atom in the adsorption configurations, while C_V reached a value of 2.85 k_B per atom. This enhancement is likely attributed to the vibrational contributions of the adsorbed gas molecules, which increase the total number of accessible vibrational modes in the system. Notably, the thermal expansion coefficient (α) showed a more significant variation. The pristine configuration exhibited $\alpha = 4.75 \times 10^{-5}$ K^{-1}, which increased to 5.16×10^{-5} K^{-1} upon NH_3 adsorption-higher than the corresponding values for CO (4.72×10^{-5} K^{-1}) and H_2S (4.96×10^{-5} K^{-1}). This pronounced change indicates a strong interaction between NH_3 molecules and WSe_2Mn lattice, highlighting both the influence of NH_3 on lattice vibrations and the high sensitivity of the material system to this particular gas.

From a dynamical perspective, the Debye temperature (T_D) serves as an indicator of the overall stiffness of the crystal lattice and is directly associated with the maximum vibrational

Table 2 Thermo-mechanical parameters of the WSe_2Mn monolayer before and after $CO/H_2S/NH_3$ gas adsorption (bulk modulus B, shear modulus G, heat capacity C_p, heat capacity C_V, thermal expansion α, Debye temperature T_D)

Configurations	B (GPa)	G (GPa)	C_p (k_B per atom)	C_V (k_B per atom)	α (K^{-1})	T_D (K)
WSe_2Mn monolayer	17.36	26.38	2.93	2.84	4.75×10^{-5}	272.28
CO adsorption	22.60	26.22	2.96	2.84	4.72×10^{-5}	272.87
H_2S adsorption	22.41	25.80	2.99	2.85	4.96×10^{-5}	261.33
NH_3 adsorption	21.28	26.30	2.97	2.85	5.16×10^{-5}	262.51

frequency of the system. For the pristine WSe_2Mn monolayer, T_D was calculated to be 272.28 K-significantly higher than that of bulk WSe_2 (160 K (ref. 45)). This enhancement can be attributed to the two-dimensional nature of the material and the local lattice stiffening induced by Mn doping. Upon adsorption of H_2S and NH_3 molecules, T_D exhibited a slight reduction to 261.33 K and 262.51 K, respectively, suggesting a softening of lattice vibrations due to gas–surface interactions.

In comparison with bulk WSe_2 ($B = 63.7$ GPa, $G = 52.5$ GPa,[46] $\alpha = 5.7 \times 10^{-5}$ K^{-1},[47] $T_D = 160$ K (ref. 45)), the Mn-doped monolayer clearly possesses lower mechanical stiffness but exhibits a Debye temperature approximately 70% higher. This behavior is characteristic of two-dimensional materials, where weak interlayer interactions along the out-of-plane (z) direction reduce resistance to compressive and shear forces, yet the restricted dimensionality leads to elevated vibrational frequencies due to limited degrees of freedom. These findings suggest that gas adsorption exerts a measurable influence on the thermo-mechanical behavior of WSe_2Mn monolayer. In particular, the observed sensitivity of the thermal expansion coefficient and Debye temperature to different adsorbed gas species highlights the potential of this material for application in gas sensing technologies, where detection may be achieved through mechanical–thermodynamic response signatures.

The electronic and magnetic properties of pristine and gas-adsorbed WSe_2Mn systems are examined *via* band structure and density of states (DOS) analyses (Fig. 2). All configurations exhibit spin-polarized semi-metallic behavior, with metallic characteristics in the spin-up channel and semiconducting features in the spin-down channel, confirming their magnetic nature. For the CO-adsorbed system, the band structure remains largely similar to that of pristine WSe_2Mn in the valence band region, but shows increased DOS above 2 eV in the conduction band. The DOS peak heights are ~11.5 states per eV for both pristine and CO-adsorbed systems, while slightly higher values are observed for H_2S (~12 states per eV) and NH_3 (~16 states per eV), indicating stronger electronic perturbations induced by these gases.

Partial DOS (PDOS) analysis (Fig. 3) reveals that Se orbitals (particularly p_x) dominate the valence band in the pristine structure, with Se(s) peaking at −4.5 eV and W/Mn(s) contributions localized deeper (~−6 eV). Upon CO adsorption, C and O states appear mainly at −4.5 eV and 2.5 eV, showing localized hybridization with Se. H_2S adsorption introduces a broader energy distribution of S states (−6.5 eV to 4 eV) and clear spin asymmetry, indicating stronger and more complex hybridization compared to CO and NH_3. In contrast, N states in the NH_3-adsorbed system are confined near −6.5 eV and −1.6 eV, suggesting limited interaction with Se.

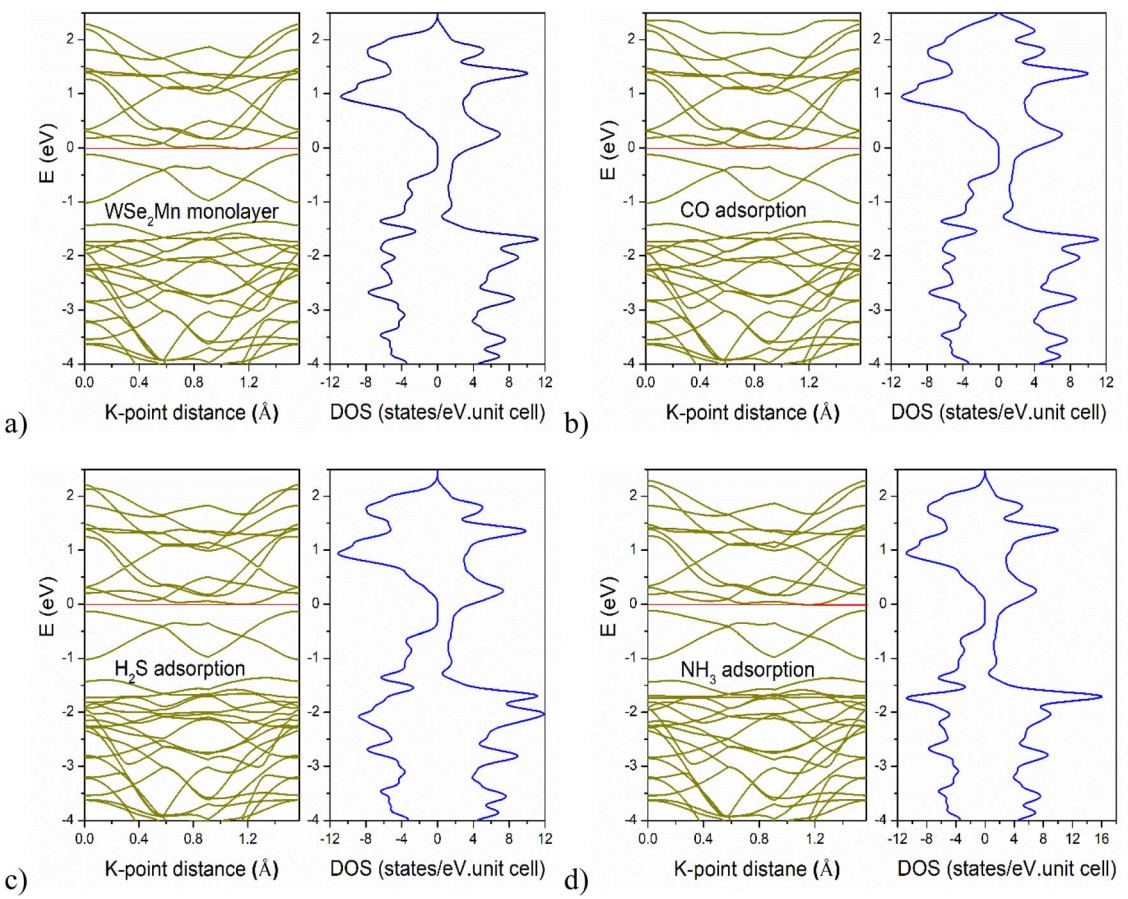

Fig. 2 Band structure and density of states of configurations: (a) pristine WSe_2Mn monolayer; (b) CO-adsorbed WSe_2Mn monolayer; (c) H_2S-adsorbed WSe_2Mn monolayer; (d) NH_3-adsorbed WSe_2Mn monolayer.

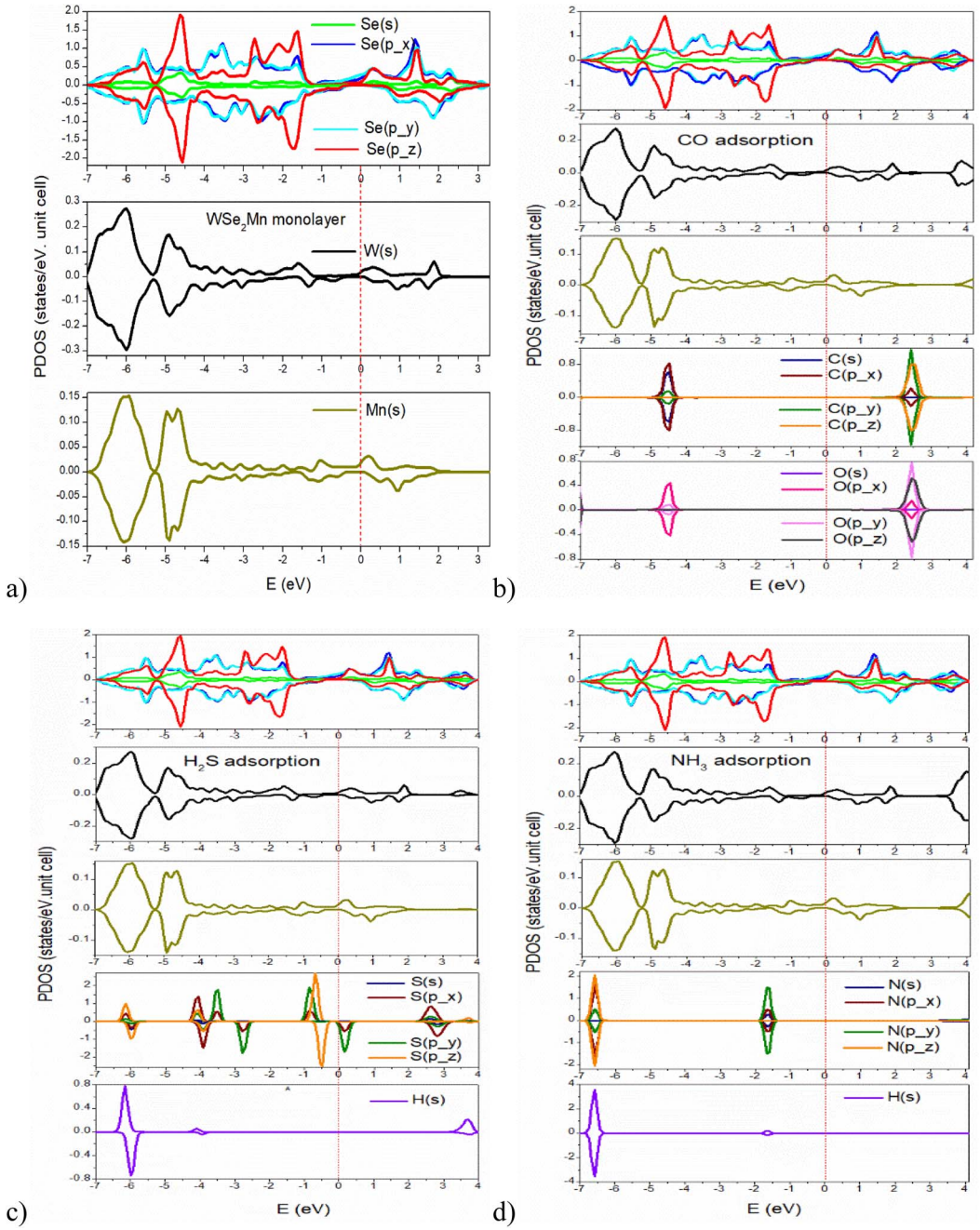

Fig. 3 Partial DOS (PDOS) of configurations: (a) pristine WSe_2Mn monolayer; (b) CO-adsorbed WSe_2Mn monolayer; (c) H_2S-adsorbed WSe_2Mn monolayer; (d) NH_3-adsorbed WSe_2Mn monolayer.

Overall, the results highlight that gas adsorption not only modifies the electronic structure of WSe_2Mn but also induces distinct spin-dependent hybridization patterns, particularly pronounced in the case of H_2S. These features may be leveraged to achieve gas-specific electronic responses in spintronic or sensing applications.

The charge density difference for the CO, H_2S, and NH_3 adsorption configurations is illustrated in Fig. 4. It is evident that gas adsorption induces a redistribution of charge around both the adsorbed molecules and WSe_2Mn surface in proximity to these molecules. The interaction between the gas molecules and the substrate is visualized through charge accumulation and depletion regions, represented by blue and yellow areas in the interfacial space. The adsorption interaction primarily occurs between the Se atoms of WSe_2Mn monolayer and the CO, H_2S, and NH_3 molecules. In contrast, the inner W and Mn atoms exhibit negligible interaction with the adsorbed species, as indicated by the minimal charge redistribution, appearing as small, dispersed yellow and blue regions around these atoms.

3.2. Optical properties

The optical properties of WSe_2Mn and its CO, H_2S, and NH_3 adsorption configurations are analyzed through the dielectric

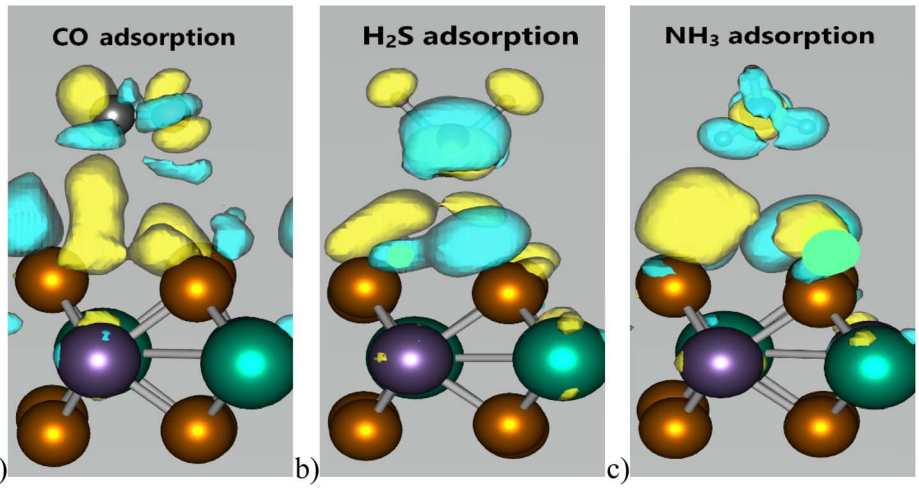

Fig. 4 The charge density difference in the configurations: (a) CO-adsorbed WSe_2Mn monolayer; (b) H_2S-adsorbed WSe_2Mn monolayer; (c) NH_3-adsorbed WSe_2Mn monolayer (the yellow region is where the charge is enhanced, the blue region is where the charge is reduced).

function (Fig. 5), absorption coefficient (Fig. 6), and electron–hole density distribution (Fig. 7). The dielectric function is presented in terms of its real and imaginary components.

As illustrated in Fig. 5, the pristine and CO-adsorbed WSe_2Mn configurations exhibit strong optical activity within the 0–8 eV energy range. In comparison, H_2S- and NH_3-adsorbed systems extend this activity slightly further, up to ~8.5 eV and ~8.3 eV, respectively, indicating enhanced optical responsiveness due to gas adsorption.

All systems show negative values in the real part of the dielectric function ($\varepsilon_1(\omega)$) along the x and y directions within certain energy ranges, implying a low-loss propagation of electromagnetic waves-an essential characteristic for optoelectronic and photonic applications. Along the z-direction, $\varepsilon_1(\omega)$ exhibits

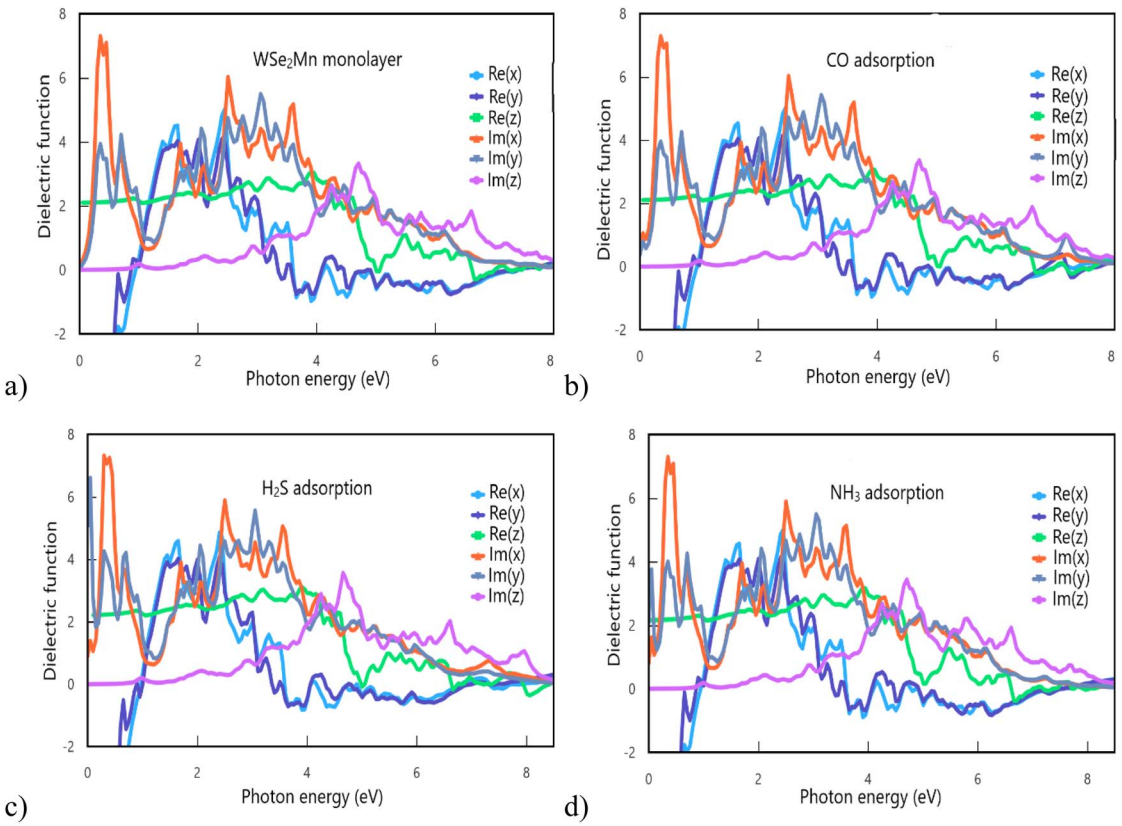

Fig. 5 Dielectric function of the configurations: (a) pristine WSe_2Mn monolayer; (b) CO-adsorbed WSe_2Mn monolayer; (c) H_2S-adsorbed WSe_2Mn monolayer; (d) NH_3-adsorbed WSe_2Mn monolayer.

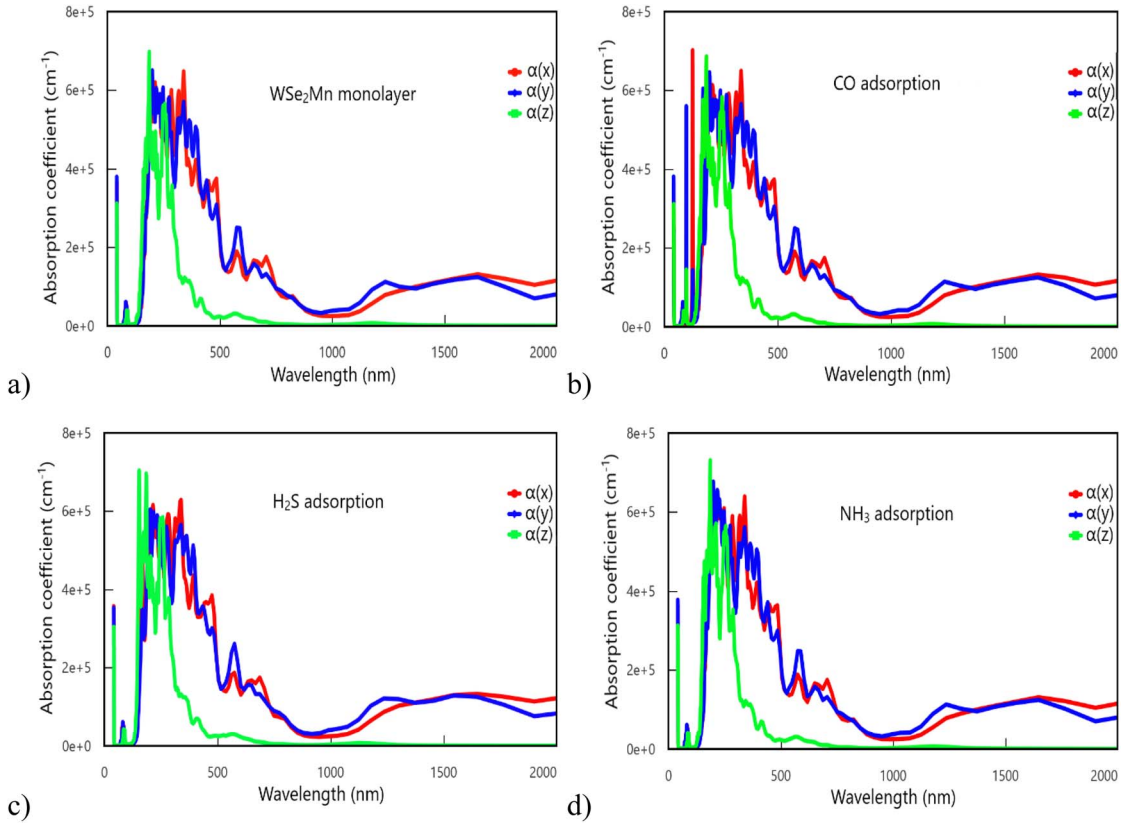

Fig. 6 Absorption coefficient of the configurations: (a) pristine WSe_2Mn monolayer; (b) CO-adsorbed WSe_2Mn monolayer; (c) H_2S-adsorbed WSe_2Mn monolayer; (d) NH_3-adsorbed WSe_2Mn monolayer.

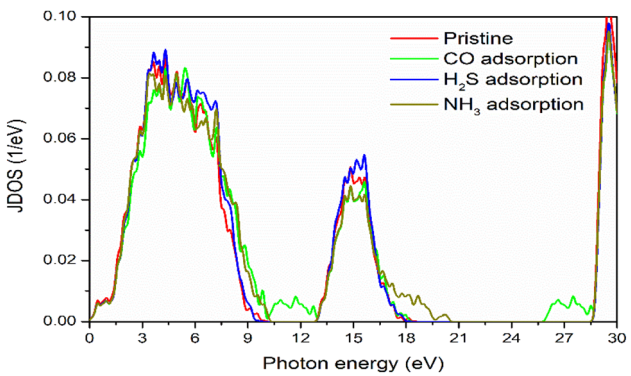

Fig. 7 The joint density of states (jDOS) of the configurations.

lower intensity due to the limited thickness of the monolayer (three atomic layers), as opposed to the infinite extent in the x–y plane.

Prominent peaks in $\varepsilon_1(\omega)$ appear near 2 eV for both the x and y directions, corresponding to the visible light region, where the material shows maximum attenuation. At higher photon energies (above ~8 eV), attenuation rapidly diminishes, indicating high transparency in the ultraviolet range. These results suggest that WSe_2Mn, particularly in gas-adsorbed forms, could be a promising candidate for tunable optoelectronic devices and optical communication components.

The imaginary part of the dielectric function $\varepsilon_2(\omega)$ reveals a pronounced anisotropy. The most intense peak is observed along the x-direction at approximately 0.3 eV, within the infrared region, suggesting significant energy dissipation due to electromagnetic wave interaction at this energy. This peak is followed by a less intense response along the y-direction, while the z-direction exhibits minimal response, indicating negligible absorption along the out-of-plane axis.

In the energy range of 0–4 eV, dominant absorption features are retained in the x- and y-directions, confirming strong in-plane interaction with incident radiation. Beyond 4 eV, $\varepsilon_2(\omega)$ gradually decreases for all directions, with convergence observed near 8 eV for the pristine and CO-adsorbed systems. For H_2S- and NH_3-adsorbed configurations, this convergence shifts slightly to ~8.5 eV. These convergence points signify a transition beyond which the material exhibits minimal electromagnetic loss, indicating transparency to higher-energy photons.

Analysis of the absorption coefficient (α) further corroborates the material's strong light–matter interaction (Fig. 6). All configurations show intense absorption in the 160–480 nm range, corresponding to ultraviolet and visible light (particularly violet and blue regions). In the investigated configurations, the maximum absorption coefficient reaches approximately 7.1 $\times 10^5$ cm^{-1} at an energy of about 6.2 eV. Compared to pristine monolayer WSe_2, which was previously reported to exhibit

a maximum absorption coefficient of around 1.6×10^6 cm^{-1} at 5.6 eV, the present results indicate a shift of the main absorption peak toward higher energy (blue-shift).[48] This shift can be attributed to the effects of doping and gas adsorption, which modify the electronic band structure and the density of states, thereby altering the resonance conditions for optical transitions. Notably, distinct anisotropic features are observed: CO adsorption induces dual peaks in the *x*- and *y*-directions, whereas H_2S adsorption leads to enhanced absorption along the *z*-axis.

At wavelengths exceeding 700 nm, absorption in the *z*-direction diminishes to nearly zero, while the *x*- and *y*-components persist at low but finite values beyond 800 nm. These findings underscore the directional dependence of light absorption in WSe_2Mn and its modified states. Overall, the pronounced anisotropic optical response and strong absorption in the UV-visible region suggest that WSe_2Mn is a promising candidate for applications in optoelectronics, sensing, photocatalysis, and biomedical technologies.

The joint density of states (jDOS) spectrum of the pristine system exhibits a prominent peak in the low-energy region (approximately 3–6 eV), with its intensity gradually diminishing as the photon energy increases (Fig. 7). This behavior suggests that the pristine material possesses a strong light absorption capability in the ultraviolet (UV) and partially visible regions, facilitating the generation of electron–hole pairs and thereby enhancing the system's conductivity. Upon CO adsorption, significant modifications in the jDOS spectrum are observed, characterized by the emergence of new peaks in the higher-energy regions (around 9–12 eV and 26–28 eV). In the case of H_2S adsorption, the jDOS intensity is notably enhanced in the mid-energy range (approximately 9–12 eV) compared to the pristine state. Conversely, NH_3 adsorption introduces subtle jDOS peaks in the high-energy region (around 18–21 eV). These alterations underscore the substantial influence of CO, H_2S, and NH_3 adsorption on the electronic structure of the material, leading to an expanded jDOS profile. This expansion in jDOS highlights the potential for utilizing these gas-adsorbed configurations in optical devices operating within high-energy regimes.

4. Conclusions

The structural, electronic, magnetic, optical, and thermo-mechanical properties of Mn-doped WSe_2 (WSe_2Mn) monolayers, both pristine and adsorbed with CO, H_2S, and NH_3 gas molecules, were systematically investigated using density functional theory (DFT) and machine learning (CGCNN) approaches. Electronic structure analysis revealed spin-resolved semimetallic behavior, characterized by a metallic spin-up channel and a semiconducting spin-down channel, which remained largely unchanged upon gas adsorption. The material's intrinsic magnetic moment was also preserved, indicating that adsorption induces minimal perturbation to its magnetic characteristics. All adsorption processes were exothermic with adsorption energies below 1 eV, confirming weak chemisorption as the dominant interaction mechanism. In terms of thermo-mechanical behavior, gas adsorption led to an increase in bulk modulus and heat capacities, while the shear modulus remained nearly constant, indicating selective stiffening under compressive strain. The thermal expansion coefficient (α) and Debye temperature (T_D) exhibited notable gas-specific variations, particularly under NH_3 exposure, suggesting enhanced vibrational coupling and mechanical–thermal sensitivity to gas adsorption. Optical analyses showed strong absorption in the ultraviolet and partial visible ranges for all configurations, supporting potential optoelectronic applications. These findings point to the potential of WSe_2Mn monolayers as multifunctional materials for use in nanoelectronic devices, gas sensors, and thermomechanical-responsive systems.

Data availability

Data supporting the findings of this study are available within the article.

Author contributions

N. V. Hoang was responsible for designing and performing the computational research, including the preparation of input files. Tr. Q. Trieu handled the organization and presentation of the results in tables and figures. Both N. V. Hoang and Tr. Q. Trieu contributed equally to drafting and editing the main manuscript. All authors participated in the review and approval of the final version.

Conflicts of interest

We declare we have no competing interests.

Acknowledgements

The authors gratefully acknowledge the support of the HPC system at the Institute for Advanced Study in Technology (IAST), Ton Duc Thang University.

References

1 G. Fiori, *et al.*, Electronics based on two-dimensional materials, *Nat. Nanotechnol.*, 2014, **9**(10), 768–779.
2 P. Miró, M. Audiffred and T. Heine, An atlas of two-dimensional materials, *Chem. Soc. Rev.*, 2014, **43**(18), 6537–6554.
3 M. Xu, *et al.*, Graphene-like two-dimensional materials, *Chem. Rev.*, 2013, **113**(5), 3766–3798.
4 S. Barth, *et al.*, Synthesis and applications of one-dimensional semiconductors, *Prog. Mater. Sci.*, 2010, **55**(6), 563–627.
5 S. V. Kuchibhatla, *et al.*, One dimensional nanostructured materials, *Prog. Mater. Sci.*, 2007, **52**(5), 699–913.
6 L. Wang, *et al.*, One-dimensional electrical contact to a two-dimensional material, *Science*, 2013, **342**(6158), 614–617.

7 Y. Ma, *et al.*, Zero-dimensional to three-dimensional nanojoining: current status and potential applications, *RSC Adv.*, 2016, **6**(79), 75916–75936.
8 J. N. Tiwari, R. N. Tiwari and K. S. Kim, Zero-dimensional, one-dimensional, two-dimensional and three-dimensional nanostructured materials for advanced electrochemical energy devices, *Prog. Mater. Sci.*, 2012, **57**(4), 724–803.
9 J. Zheng, *et al.*, Advanced anode materials of potassium ion batteries: from zero dimension to three dimensions, *Nano-Micro Lett.*, 2021, **13**, 1–37.
10 D. Abergel, *et al.*, Properties of graphene: a theoretical perspective, *Adv. Phys.*, 2010, **59**(4), 261–482.
11 L. Falkovsky and S. Pershoguba, Optical far-infrared properties of a graphene monolayer and multilayer, *Phys. Rev. B: Condens. Matter Mater. Phys.*, 2007, **76**(15), 153410.
12 Q. Lu, M. Arroyo and R. Huang, Elastic bending modulus of monolayer graphene, *J. Phys. D: Appl. Phys.*, 2009, **42**(10), 102002.
13 D. Chung, Review graphite, *J. Mater. Sci.*, 2002, **37**, 1475–1489.
14 D. Chung, A review of exfoliated graphite, *J. Mater. Sci.*, 2016, **51**, 554–568.
15 H. Dai, Carbon nanotubes: opportunities and challenges, *Surf. Sci.*, 2002, **500**(1–3), 218–241.
16 V. N. Popov, Carbon nanotubes: properties and application, *Mater. Sci. Eng., R*, 2004, **43**(3), 61–102.
17 F. Giacalone and N. Martin, Fullerene polymers: synthesis and properties, *Chem. Rev.*, 2006, **106**(12), 5136–5190.
18 F. Wudl, Fullerene materials, *J. Mater. Chem.*, 2002, **12**(7), 1959–1963.
19 W.-T. Hsu, *et al.*, Evidence of indirect gap in monolayer WSe_2, *Nat. Commun.*, 2017, **8**(1), 929.
20 J.-K. Huang, *et al.*, Large-area synthesis of highly crystalline WSe_2 monolayers and device applications, *ACS Nano*, 2014, **8**(1), 923–930.
21 R. Zhao, *et al.*, First-Principle Study of Bandgap Engineering and Optical Properties of Monolayer WSe_2 in Second Near-Infrared Windows, *Adv. Mater. Interfaces*, 2023, **10**(23), 2300277.
22 D. Muoi, *et al.*, Electronic properties of WS_2 and WSe_2 monolayers with biaxial strain: a first-principles study, *Chem. Phys.*, 2019, **519**, 69–73.
23 W. Liu, *et al.*, High-performance field-effect-transistors on monolayer-WSe_2, *ECS Trans.*, 2013, **58**(7), 281.
24 B. Liu, *et al.*, Chemical vapor deposition growth of monolayer WSe_2 with tunable device characteristics and growth mechanism study, *ACS Nano*, 2015, **9**(6), 6119–6127.
25 Y. Gao, *et al.*, Ultrafast growth of high-quality monolayer WSe_2 on Au, *Adv. Mater.*, 2017, **29**(29), 1700990.
26 H.-Y. Chen, *et al.*, Locally Doped Transferred Contacts for WSe_2 Transistors, *ACS Appl. Electron. Mater.*, 2024, **6**(11), 8319–8327.
27 S. Chen, *et al.*, Extension Doping with Low-Resistance Contacts for P-Type Monolayer WSe_2 Field-Effect Transistors, *Adv. Electron. Mater.*, 2024, 2400843.
28 Y.-R. Liu, *et al.*, Sn-doped induced stable 1T-WSe_2 nanosheets entrenched on N-doped carbon with extraordinary half/full sodium/potassium storage performance, *Rare Met.*, 2023, **42**(5), 1557–1569.
29 E. Pavoni, *et al.*, First principles study of WSe_2 and the effect of V doping on the optical and electronic properties, *Mater. Adv.*, 2024, **5**(6), 2230–2237.
30 S. Tiwari, *et al.*, Reduction of Magnetic Interaction Due to Clustering in Doped Transition-Metal Dichalcogenides: A Case Study of Mn-, V-, and Fe-Doped WSe_2, *ACS Appl. Mater. Interfaces*, 2024, **16**(4), 4991–4998.
31 A. Kagkoura, *et al.*, Cobalt-and Nickel-Doped WSe_2 as Efficient Electrocatalysts for Water Splitting and as Cathodes in Hydrogen Evolution Reaction Proton Exchange Membrane Water Electrolysis, *J. Phys. Chem. C*, 2025, **129**, 2893–2903.
32 S. Cheng, *et al.*, The adsorption and sensing mechanism of toxic gases HCN, NO_2, NH_3 and Cl_2 on Mo, Ag-modified WSe_2 monolayer: Insights from the first-principles computations, *Mater. Today Commun.*, 2023, **35**, 105906.
33 A. Kushwaha and N. Goel, A DFT study of superior adsorbate-surface bonding at Pt-WSe_2 vertically aligned heterostructures upon NO_2, SO_2, CO_2, and H_2 interactions, *Sci. Rep.*, 2024, **14**(1), 15708.
34 L. Lin, *et al.*, Adsorption of NO_2, SO_2, H_2S, and NH_3 on Os-Doped WSe_2 Monolayers: A First-Principles Study, *Langmuir*, 2023, **39**(42), 15142–15151.
35 M. Dong, *et al.*, A Study Based on the First-Principle Study of the Adsorption and Sensing Properties of Mo-Doped WSe_2 for N_2O, CO_2, and CH_4, *Chemosensors*, 2024, **12**(9), 192.
36 S. Sarkar, *et al.*, DFT analysis of Re-modified WSe_2 monolayers for adsorption of CO, C_2H_2, and C_2H_4, *Modell. Simul. Mater. Sci. Eng.*, 2024, **32**(7), 075003.
37 Z. Cui, *et al.*, Highly sensitive and selective defect WS_2 chemical sensor for detecting HCHO toxic gases, *Sensors*, 2024, **24**(3), 762.
38 Z. Cui, *et al.*, Adsorption of CO, NH_3, NO, and NO_2 on pristine and defective g-GaN: Improved gas sensing and functionalization, *Appl. Surf. Sci.*, 2020, **530**, 147275.
39 Z. Cui, *et al.*, Adsorption of gas molecules on intrinsic and defective $MoSi_2N_4$ monolayer: Gas sensing and functionalization, *Sens. Actuators, A*, 2024, **366**, 114954.
40 Z. Cui, *et al.*, Toxic gas molecules adsorbed on intrinsic and defective WS_2: gas sensing and detection, *Appl. Surf. Sci.*, 2023, **613**, 155978.
41 Y. Qin, T. Zhang and Z. Cui, Core-shell structure of polypyrrole grown on $W_{18}O_{49}$ nanorods for high performance gas sensor operating at room temperature, *Org. Electron.*, 2017, **48**, 254–261.
42 M. Monshi, S. Aghaei and I. Calizo, Edge functionalized germanene nanoribbons: impact on electronic and magnetic properties, *RSC Adv.*, 2017, **7**(31), 18900–18908.
43 C. Li, *et al.*, Bandgap engineering of monolayer MoS_2 under strain: A DFT study, *J. Korean Phys. Soc.*, 2015, **66**, 1789–1793.
44 M. Pumera and C. H. A. Wong, Graphane and hydrogenated graphene, *Chem. Soc. Rev.*, 2013, **42**(14), 5987–5995.
45 S. Mathew, *et al.*, Temperature dependent structural evolution of WSe_2: A synchrotron X-ray diffraction study, *Condens. Matter*, 2020, **5**(4), 76.

46 L.-p. Feng, *et al.*, Effect of pressure on elastic, mechanical and electronic properties of WSe_2: A first-principles study, *Mater. Res. Bull.*, 2014, **50**, 503–508.
47 T. M. Kucinski, *et al.*, Direct Measurement of the Thermal Expansion Coefficient of Epitaxial WSe_2 by Four-Dimensional Scanning Transmission Electron Microscopy, *ACS Nano*, 2024, **18**(27), 17725–17734.
48 H.-L. Liu, *et al.*, Temperature-dependent optical constants of monolayer MoS_2, $MoSe_2$, WS_2, and WSe_2: spectroscopic ellipsometry and first-principles calculations, *Sci. Rep.*, 2020, **10**(1), 15282.